

Schottky–Mott limit in graphene inserted 2D semiconductor–metal interfaces

Cite as: J. Appl. Phys. **132**, 145301 (2022); <https://doi.org/10.1063/5.0106620>

Submitted: 29 June 2022 • Accepted: 10 September 2022 • Published Online: 10 October 2022

 Sanchali Mitra and  Santanu Mahapatra



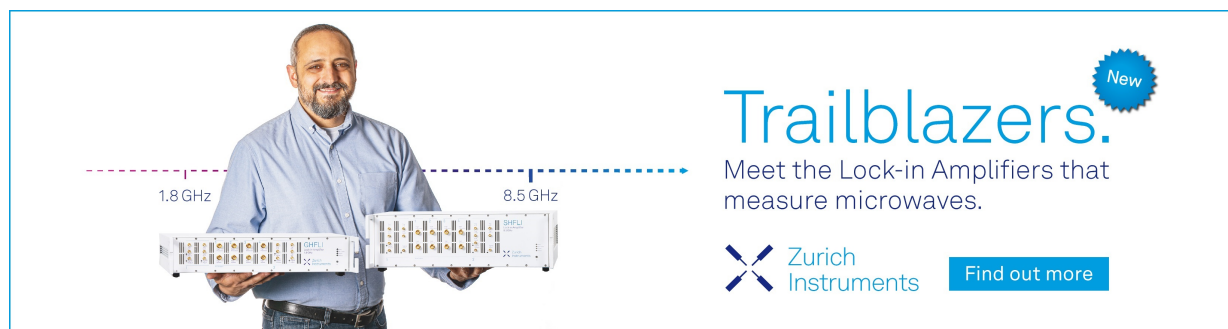
View Online



Export Citation



CrossMark



Trailblazers. 

Meet the Lock-in Amplifiers that measure microwaves.

 Zurich Instruments [Find out more](#)

Schottky–Mott limit in graphene inserted 2D semiconductor–metal interfaces

Cite as: J. Appl. Phys. **132**, 145301 (2022); doi: [10.1063/5.0106620](https://doi.org/10.1063/5.0106620)

Submitted: 29 June 2022 · Accepted: 10 September 2022 ·

Published Online: 10 October 2022



View Online



Export Citation



CrossMark

Sanchali Mitra  and Santanu Mahapatra^{a)} 

AFFILIATIONS

Nano-Scale Device Research Laboratory, Department of Electronic Systems Engineering,
Indian Institute of Science (IISc) Bangalore, Bangalore 560012, India

^{a)}Author to whom correspondence should be addressed: santanu@iisc.ac.in

ABSTRACT

The insertion of a graphene (or h-BN) layer in a two-dimensional (2D) MoS₂–metal interface to de-pin the Fermi level has been a common strategy in experiments. Recently, however, the 2D material space has expanded much beyond transition metal dichalcogenides, and it is not clear if the same strategy will work for other materials. Here, we select a family of twelve emerging, commercially available 2D semiconductors with the work function range of 3.8–6.1 eV and study their interfaces with metals in the presence and absence of the graphene buffer layer. Using the density functional theory, we show that the graphene buffer layer preserves the ideal Schottky–Mott rule to a great extent when the interfaces are made with Ag and Ti. However, the h-BN buffer layer does not yield a similar performance since its electrons are not as localized as graphene. It is further observed that even graphene is not very effective in preserving the ideal Schottky–Mott rule while interfacing with high work function metals (Au, Pd, and Pt). The quantum chemical insights presented in this paper could aid in the design of high-performance electronic devices with low contact resistance based on newly developed 2D materials.

Published under an exclusive license by AIP Publishing. <https://doi.org/10.1063/5.0106620>

I. INTRODUCTION

After the first successful synthesis of graphene in 2004,¹ these two-dimensional materials have opened a new door to building high-performance devices beyond the limit of traditional silicon technology.^{2–4} The heterostructures formed by contacting 2D semiconductors (SCs) with bulk metals or other 2D materials possess several advantages, like atomic-scale thickness, ultrafast charge transfer, scaling flexibility, and tunable bandgap.^{5–7} In the last decade, 2D transition metal dichalcogenides (TMD), mostly MoS₂, have been extensively studied for their application in nano-electronic devices.^{8–11} However, the devices usually suffer from high contact resistance, resulting in a much lower drain current than the desired value required for high-performance applications.^{12,13} Due to the Fermi level (FL) pinning (FLP),^{14–16} it is very difficult to mitigate the contact resistance by changing electrode materials. Buffer layer insertion between the metal and 2D TMD are reported to be an effective strategy for weakening FLP.¹⁷ 2D materials such as graphene and hexagonal boron nitride (h-BN) are prospective buffer layers due to the atomic thickness, easy deposition, and van der Waals interactions with the TMD materials.^{17,18} Most theoretical and experimental works on buffer layer insertion

have been performed on MoS₂ based devices.^{19–24} However, as the 2D material library is growing every year, newly emerged 2D materials are gaining attention for their potential applications.²⁵ Some works have already been reported on developing field effect transistors from different 2D families such as metal monochalcogenides (SnS)²⁶ and novel metal dichalcogenides (PdSe₂/PtSe₂),²⁷ and mono-elemental materials such as phosphorene²⁸ and tellurene.²⁹ Recently, it was shown that monolayer (ML) tellurene suffers from metallization when in contact with any metals.³⁰ Inserting graphene can prevent metallization and create a Schottky barrier whose height can be modulated by changing electrode materials. Direct metal contacts of ML phosphorene³¹ and SnS³² also show metallization of the SC, restricting their use in vertical Schottky devices. However, the strategy for FL depinning in the 2D materials other than MoS₂ has not been well studied.

In this work, we investigated the effect of buffer layer insertion in the metal contacts of a series of emerging 2D semiconducting materials. We have selected twelve commercially available 2D SCs with a wide range of work functions (WFs) (3.8–6.1 eV). Using rigorous DFT calculations, we have evaluated the electronic properties of their interfaces with metals in the presence and absence of

buffer layers. Ag and Ti are initially selected as electrode materials as their WFs are nearly equal but chemical reactivity is different. Comparing the obtained barrier properties with the traditional Schottky–Mott (SM) rule, we have made a comparative analysis between the performance of ML graphene and h-BN as the buffer layer with these two metals. Furthermore, we have evaluated how the barrier properties change when metals with high WF are used as electrode materials. For the first time, the buffer insertion strategy is evaluated in a series of 2D materials apart from MoS₂. The insights provide the selection of a suitable combination of the buffer layer and metal electrodes to build heterostructures that can approach the SM limit.

II. CALCULATION DETAILS

The geometry optimizations were performed by using the projected augmented wave method (PAW)³³ as implemented in Vienna *Ab-initio* Simulation Package (VASP).^{34,35} Generalized gradient approximation (GGA) with Perdew–Burke–Ernzerhof (PBE)³⁶ functional and van der Waals correction proposed by the Grimme DFT-D3^{37,38} method has been used. A cutoff energy of 520 eV and $\frac{30}{a} \times \frac{30}{b} \times 1$ Monkhorst–Pack³⁹ k-points grids were used, where *a*, *b*, and *c* are the lengths of the lattice parameters of a supercell. The Gaussian smearing method with a smearing width of 0.05 eV was used. As the self-convergence criteria, the energy difference in successive iterations was set to 10^{−6} eV. The geometry was optimized until the force on every atom falls below 0.05 eV/Å. Dipole correction is applied to eliminate the pseudo-interaction of the dipole moments due to the periodicity in the *z*-direction.

In the work on tellurene heterostructures,³⁰ some discrepancies between the projected band structures calculated using plane wave basis and localized orbital basis have been reported. To calculate projected states, the wave function is projected onto localized atomic orbitals. For the projection calculation using a plane wave basis set, some projection loss may arise as the radius of a sphere around the atom is set to cut off the projection. As in localized orbital basis, there is no need for approximating a sphere around the atom, the projection calculation should be more accurate than plane wave basis. Therefore, for the calculations of electronics properties, we have used QuantumATK-atomistic simulation software⁴⁰ that uses a linear combination of atomic orbital (LCAO) basis sets. The accuracy of the basis set was set to “medium,” and SG15 norm-conserving pseudopotentials^{41,42} were used. van der Waals interactions with the zero damping DFT-D3 method of Grimme were employed. A cutoff energy of 185 Ha and a denser *k* mesh $\frac{60}{a} \times \frac{60}{b} \times 1$ were chosen for these static calculations. The Gaussian smearing method with a temperature of 600 K was used. For the interface design, six layers of the ⟨111⟩-cleaved surface of Ag and the ⟨0001⟩-cleaved surface of Ti were considered. The interfaces were created using the QuantumATK interface builder module.⁴³ To create an interface, initially, the supercells of two surfaces were aligned. Strain was then applied on one or both surfaces to match the aligned supercells. As significant strain can alter the material properties, the supercell size should be increased to reduce the lattice mismatch. Therefore, in this work, we have used sufficiently large supercells to keep the interface strain below 1%. To build the buffer inserted heterostructures, first, the interfaces between the

metal and buffer layer were created by applying strain on both surfaces. 2D SCs were then interfaced with the formed 2D buffer (graphene/h-BN)–metal surfaces. All the details regarding the interface building, including the applied strain, supercell size, surface rotation angle, are given in Tables S1 and S2 in the [supplementary material](#). A vacuum layer of 20 Å was added for DFT calculations to eliminate any pseudo-interaction between two periodic replicas. During geometry relaxations, the top three layers of the metal toward the vacuum side were fixed to emulate the bulk electrode feature. The semiconductor atoms are free to move. Therefore, any strain in the semiconductor layer while making contact is automatically introduced during geometry relaxations.

III. RESULTS AND DISCUSSIONS

A. Graphene insertion

1. Interface geometries

We randomly selected twelve commercially available 2D materials with WFs ranging from 3.8 to 6.1 eV. From monochalcogenides group, SnS, GeSe, PbTe, GaTe, InSe, and InTe are used; from dichalcogenides, WTe₂, WSe₂, PdSe₂, PtSe₂, and SnS₂ are selected; and from M₂X₃ group, Sb₂S₃ is taken. At the equilibrium state, ML SnS, GeSe, and PbTe have a space group symmetry Pmn2₁, with an anisotropic structure in which a Sn(Ge/Pb) or S (Se/Te) atom is covalently bonded to three S(Se/Te) or Sn(Ge/Pb) atoms. In WTe₂ and WSe₂, W and Te(Se) atoms are arranged periodically in hexagonal symmetry. ML GaTe, InTe, and InSe have four covalently bonded atomic planes in Te(Se)–Ga(In)–Ga(In)–Te(Se) sequence. PtSe₂, PdSe₂, and SnS₂ have T phases with the P-3m1 group in which each Pt(Pd/Sn) atom is encompassed by six Se (S) atoms. In the crystal structure of Sb₂S₃, each Sb atom is surrounded by six S atoms and four Sb atoms surround each S atom. The top view and side view images of the atomic structures of these materials are shown in Fig. 1(a). The lattice parameters are mentioned in the figure caption. Among the 2D materials, SnS has the lowest WF of about 3.87 eV, and SnS₂ has the highest of about 6.09 eV [Fig. 1(b)]. The WFs are calculated using the ghost atom technique in QuantumATK. In Fig. 1(b), the schematic representations of band diagrams of the 2D materials are shown. The energy values of conduction band minima (CBM) and valence band maxima (VBM) are given in the figure. The calculated WFs and bandgaps of all the materials are given in Table S3 in the [supplementary material](#).

To evaluate the electronic properties of 2D SC–metal systems, the interfaces of these materials with Ag and Ti are formed. We chose Ag and Ti primarily as their WFs are nearly equal, but most of the 2D materials are physisorbed on Ag while chemisorbed on Ti. Ti is more reactive due to partially filled d-orbitals. The relaxed geometries of the interfaces of GeSe and WSe₂ are depicted in Fig. 2. The structural parameters are listed in Table I. The average interlayer distances between 2D materials and metal surfaces are in the range of 2.5–3 and 1.5–2.5 Å for 2D SC–Ag and 2D SC–Ti interfaces, respectively. These distances are comparable with the sum of covalent radii of metal atoms and neighboring 2D SC atoms, implying the formation of chemical bonds between the two. While interfacing with Ti, there is a slight distortion in the

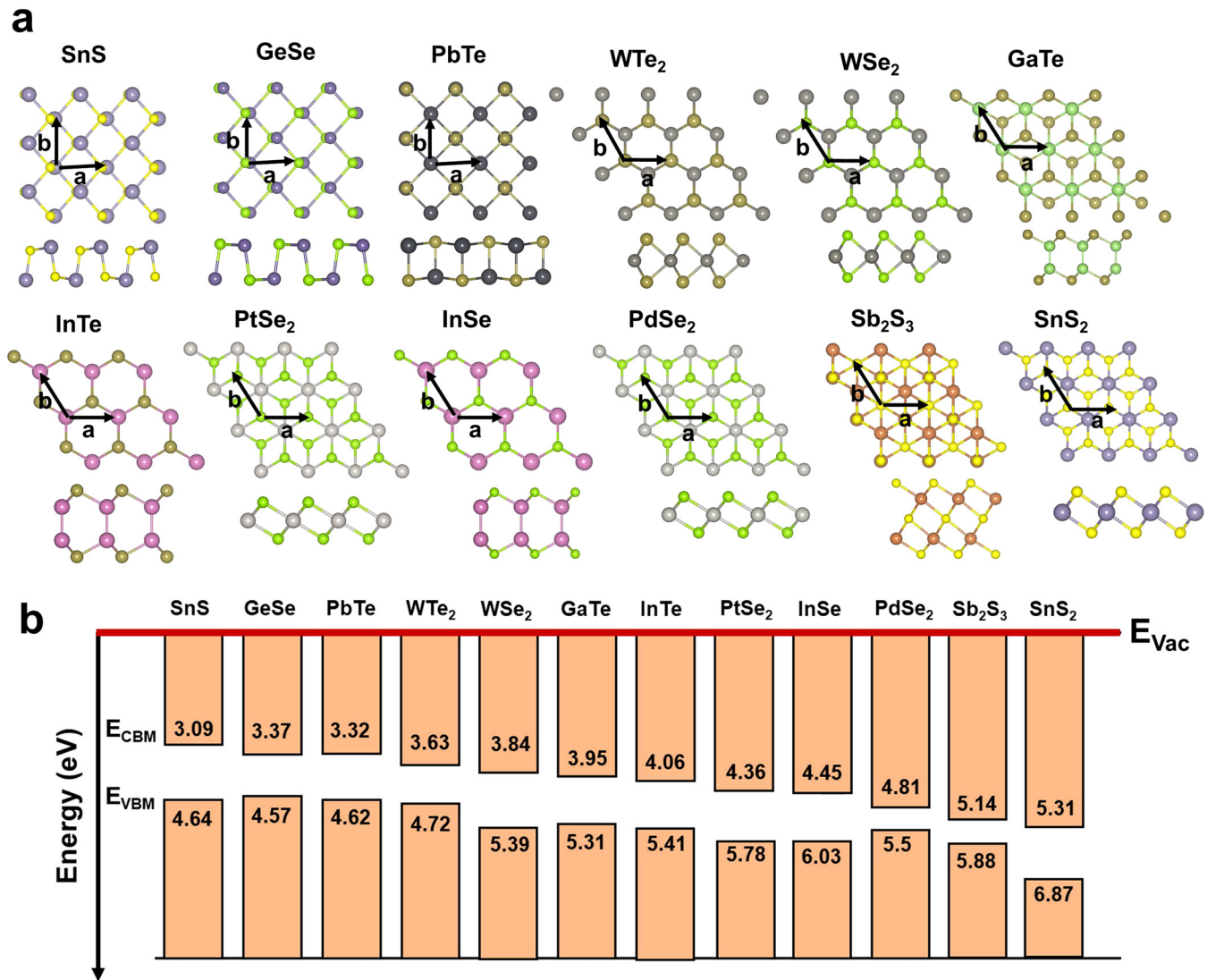


FIG. 1. (a) Top and side view images of crystal structures of the ML 2D SC. The lattice parameters are $a = 4.325 \text{ \AA}$, $b = 4.064 \text{ \AA}$ (SnS); $a = 4.274 \text{ \AA}$, $b = 3.973 \text{ \AA}$ (GeSe); $a = b = 4.64 \text{ \AA}$ (PbTe); $a = b = 3.55 \text{ \AA}$ (WTe₂); $a = b = 3.32 \text{ \AA}$ (WSe₂); $a = b = 4.13 \text{ \AA}$ (GaTe); $a = b = 4.37 \text{ \AA}$ (InTe); $a = b = 3.75 \text{ \AA}$ (PtSe₂); $a = b = 4.07 \text{ \AA}$ (InSe); $a = b = 3.73 \text{ \AA}$ (PdSe₂); $a = b = 3.92 \text{ \AA}$ (Sb₂S₃); and $a = b = 3.69 \text{ \AA}$ (SnS₂). (b) Schematic representation of band diagrams of the 2D materials. The energy values of CBM and VBM are mentioned for each material. The solid red line denotes the vacuum level.

structures of WSe₂, WTe₂, and GaTe. However, the rest of the materials are completely distorted. But with Ag, only minor structural distortion is observed. The average binding energy values of Ag adsorbed structures are much lower than Ti, implying strong chemical reactions of the 2D materials with Ti.

The average binding energy is defined as

$$\begin{aligned} E_b^{2D-M} &= [E_{2D-M} - E_{2D} - E_M]/N, \\ E_b^{2D-C-M} &= [E_{2D-C-M} - E_{2D} - E_C - E_M]/N, \end{aligned} \quad (1)$$

where E_{2D-M} , E_{2D-C-M} , E_{2D} , E_C , E_M denote the total energies of 2D-metal systems, 2D-graphene-metal systems, pure 2D materials, pure graphene, and pure metal surfaces, respectively. N is the number of atoms in the topmost layer of 2D materials that are in direct contact with metal or graphene atoms.

The chemical interactions between metal and 2D SC can be shielded by inserting a buffer layer between the two. Figure 2 shows the relaxed geometries of ML graphene inserted GeSe-metal and WSe₂-metal interfaces. The structures of 2D materials remain unchanged in both graphene-Ag and graphene-Ti systems. The

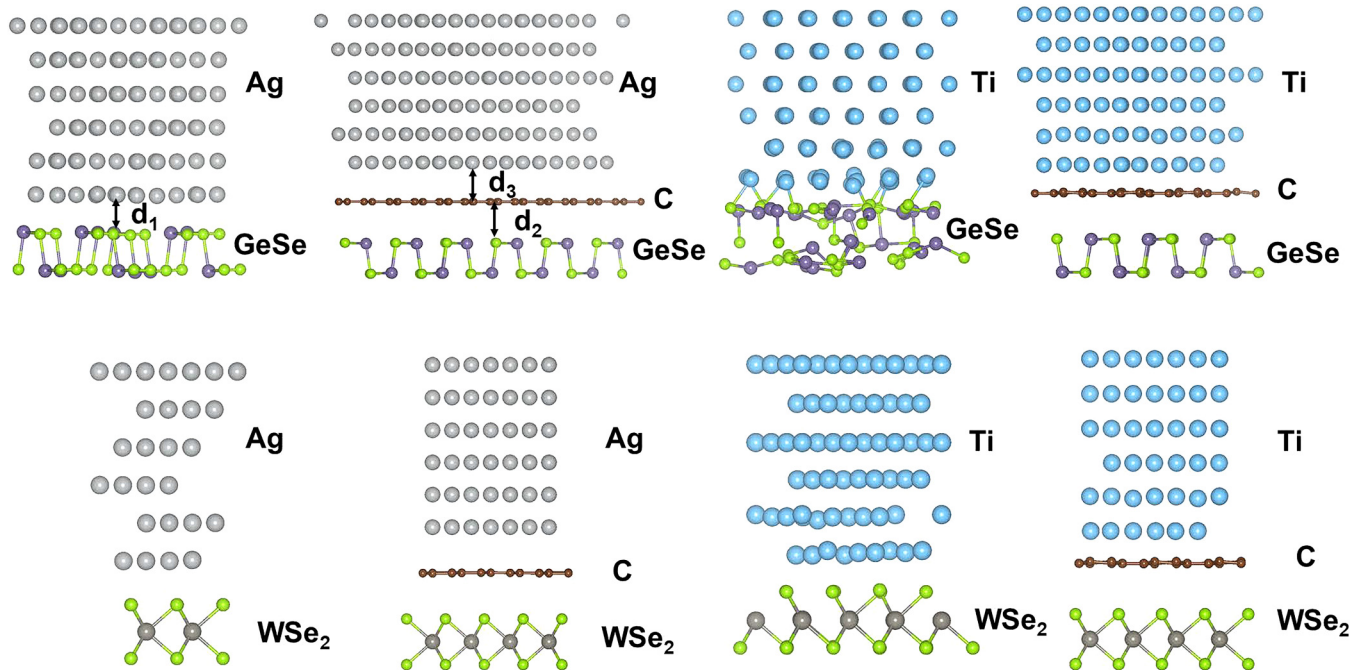


FIG. 2. Side view images of atomic structures of ML GeSe–Ag, GeSe–graphene–Ag, GeSe–Ti, and GeSe–graphene–Ti; WSe₂–Ag, WSe₂–graphene–Ag, WSe₂–Ti, and WSe₂–graphene–Ti heterostructures.

interplanar distances between 2D materials and graphene are around 3.5 Å that are much higher than the 2D–metal distances. These large distances and structural uniformity of 2D materials suggest van der Waals interactions between 2D materials and graphene. For the graphene–metal region, the interlayer distances between graphene and Ag are around 3.3 Å, while for graphene and Ti, the spacings are reduced to around 2.1 Å. The short

interlayer distances are comparable to the sum of covalent radii of Ti and C atoms. The binding energies for the graphene–Ti system are much higher than that of graphene–Ag systems (Table 1). Graphene also suffers from minor structural deformation at Ti surfaces. From the projected band analysis (Fig. S1 in the supplementary material), it is also found that the Dirac point of graphene is somehow preserved in the graphene–Ag interface.

TABLE I. Interlayer properties of 2D SC–metal (Ag/Ti) and 2D SC–graphene–metal (Ag/Ti) interfaces. d_1 , d_2 , and d_3 are the average vertical distances between 2D–metal, 2D–graphene, and graphene–metal, respectively. E_b is the calculated average binding energy using Eq. (1).

2D material	Ag interface		C–Ag interface			Ti interface		C–Ti interface		
	d_1 (Å)	E_b (eV)	d_2 (Å)	d_3 (Å)	E_b (eV)	d_1 (Å)	E_b (eV)	d_2 (Å)	d_3 (Å)	E_b (eV)
SnS	2.78	−0.53	3.56	3.37	−0.39	1.57	−2.68	3.42	2.11	−1.49
GeSe	2.63	−0.58	3.45	3.28	−0.39	1.96	−2.12	3.47	2.13	−1.36
PbTe	2.68	−0.76	3.52	3.26	−0.48	1.90	−1.90	3.54	2.18	−1.69
WTe ₂	2.86	−0.73	3.45	3.17	−0.64	2.41	−1.22	3.39	2.19	−1.92
WSe ₂	2.78	−0.63	3.39	3.35	−0.49	2.51	−1.07	3.40	2.17	−1.53
GaTe	2.75	−0.8	3.56	3.31	−0.65	2.31	−3.28	3.85	2.20	−2.24
InTe	2.72	−1.09	3.44	3.21	−0.70	2.35	−2.17	3.57	2.21	−2.59
PtSe ₂	2.53	−0.95	3.24	3.20	−0.57	1.84	−2.35	3.62	2.14	−1.92
InSe	2.65	−0.73	3.29	3.19	−0.62	1.95	−4.06	3.57	2.19	−2.27
PdSe ₂	2.44	−1.1	3.27	3.23	−0.74	1.85	−3.83	3.23	2.16	−1.92
Sb ₂ S ₃	2.52	−0.8	3.27	3.13	−0.65	1.64	−4.7	3.56	2.19	−2.14
SnS ₂	2.28	−0.86	3.31	3.24	−0.55	1.56	−5.92	3.32	2.18	−1.85

However, the band structure of graphene completely distorts while interfacing with Ti. The small interlayer separations, higher binding energy, structural deformations, and band distortion suggest graphene is chemisorbed on Ti while Ag is physisorbed.

B. Projected band analysis

The 2D materials selected in our work have bandgaps ranging from 0.6 to 1.6 eV [Fig. 1(b)]. In Fig. 3, the projected band structures of 2D materials on Ag and Ti electrodes are shown. The semiconducting band structures of all the 2D materials are destroyed on both Ag and Ti, implying chemical or covalent bonding between them. The band hybridizations of 2D materials on Ti [Fig. 3(b)] are more intense than those on Ag [Fig. 3(a)]. In all the 2D materials, some bands cross the FL leading to metallization of the 2D materials.

When graphene is inserted, the chemical interactions between the 2D SCs and metal are shielded. As a result, the semiconducting band structures of the 2D materials are restored (Fig. 4). It is found that the projected bands of 2D SC in graphene inserted interfaces are similar to those of the pristine 2D SC. It confirms the weak van der Waals interactions between ML 2D SC and graphene-metal contact regions. However, the bandgaps have slightly deviated from the pristine 2D SC, and the bands are shifted with respect to the FL due to the interlayer charge transfer. The vertical Schottky barrier height (SBH) is determined by the energy difference between the FL of the 2D SC–graphene–metal contact and the CBM (n-type Schottky barrier) or VBM (p-type Schottky barrier) of 2D SC in the graphene inserted interface. For SnS, GeSe, and PbTe contacted with the graphene–Ag surface, the FLs shift toward the VBM, creating p-type Schottky barriers [Fig. 4(a)]. The hole SBHs (Φ_p) are found to be 0.4, 0.25, and 0.18 eV, respectively. In the case of WTe₂, WSe₂, GaTe, and InTe, the FLs are adjacent to CBM indicating n-type Schottky contacts with electron SBH (Φ_n) of about 0.38, 0.68, 0.63, and 0.25 eV, respectively. For the rest of the five materials, PtSe₂, InSe, PdSe₂, Sb₂S₃, and SnS₂, the FLs shift inside the conduction band region resulting in the disappearance of vertical Schottky barriers.

As the metal electrode remains the same for all materials, the FL shift occurs according to the WF of the 2D SC. As the WF of the 2D materials increase, the barriers have gradually changed from p-type to n-type. However, the change in barrier height does not follow a linear relationship with respect to the 2D WFs as the bandgaps of the materials are different. In the case of graphene–Ti surface also, SnS, GeSe, and PbTe form p-type barrier with hole SBH 0.5, 0.5, and 0.15 eV, while WTe₂, WSe₂, GaTe, and InTe create n-type barrier with electron SBH of about 0.35, 0.5, 0.4, and 0.1 eV, respectively [Fig. 4(b)].

C. Schottky barrier analysis

In an ideal metal–semiconductor (MS) junction, the contact nature and barrier height can be well predicted by the SM rule. According to the SM rule, if the metal WF is less than the SC's CBM or greater than the VBM, the barrier height will be zero creating an Ohmic contact. If metal WF falls within the bandgap of

the SC, a Schottky contact is formed. SBH can be evaluated by

$$\phi_n = E_c - \varphi_M, \quad \phi_p = \varphi_M - E_v, \quad (2)$$

where ϕ_n and ϕ_p represent electron and hole SBH, respectively. φ_M is the WF of metal and E_c and E_v denote the CBM and VBM of the semiconductor. Band alignment follows the SM rule if no charge redistributions occur during the formation of the MS interface. Therefore, the SM rule holds for chemically non-interacting interfaces only.⁴⁴ If the chemical reaction between two materials is significantly high, FLP occurs at their interface, where the SM theory completely fails. The lower the FLP, the lower the deviation from the SM rule. DFT calculations can capture the chemical reactions between two materials. As mentioned in Sec. III B, from DFT calculated band diagrams, the SBH can be evaluated using the following equation:

$$\phi_n = E_F - E_c, \quad \phi_p = E_v - E_F, \quad (3)$$

where E_F is the FL of the MS junction after the contact is formed. Therefore, comparing the DFT calculated barrier properties [Eq. (3)] with the SM calculations [Eq. (2)], we can find out the effect of buffer layer insertion in FL depinning.

1. Barrier analysis in 2D SC–graphene–Ag heterostructures

For 2D SC–graphene–metal systems, the metal WF should be replaced by the WF of the graphene–metal system to calculate the barrier height from the SM rule. Figure 5(a) shows the comparison between the contact nature and barrier height in 2D SC–graphene–Ag heterostructures obtained from projected band structures and the SM rule. The WF of the graphene–Ag system is obtained to be 4.27 eV. We have also included the band diagrams for ML tellurene and phosphorene in this plot. The calculations for ML tellurene have been described in detail in Ref. 30. In both methods, SnS, GeSe, and PbTe form the same p-type contacts with the graphene–Ag surface. For SnS and GeSe, the electron (1.15/1.175 eV) and hole SBH (0.4/0.375 eV) are almost similar in the two methods. For PbTe, the electron and hole SBH obtained from band analysis are about 0.2 eV lower than those calculated from the SM rule. When PbTe is contacted with graphene–Ag, the bandgap of PbTe is reduced from its pristine value. For WTe₂ and tellurene, the barrier polarity is reversed in the two methods. The contact of WTe₂ with graphene–Ag electrode changes from n-type with a smaller electron SBH of 0.38 eV (band structure calculations) to p-type with the larger electron SBH of 0.635 eV (SM rule). The hole SBHs are nearly equal in both methods. On the other hand, tellurene with graphene–Ag changes from the p-type Schottky contact with smaller hole SBH of 0.65 eV (band structure calculations) to n-type contact with larger hole SBH of 1.065 eV (the SM rule). For phosphorene, both methods show the formation of the n-type Schottky contact with a small difference of about 0.1 eV in the barrier heights. WSe₂, GaTe, and InTe form an n-type contact with graphene–Ag in both the methods. However, the electron SBH is about 0.25 eV (WSe₂) and 0.3 eV (GaTe) larger in band structure calculations as compared to the SM rule. For InTe, the barrier

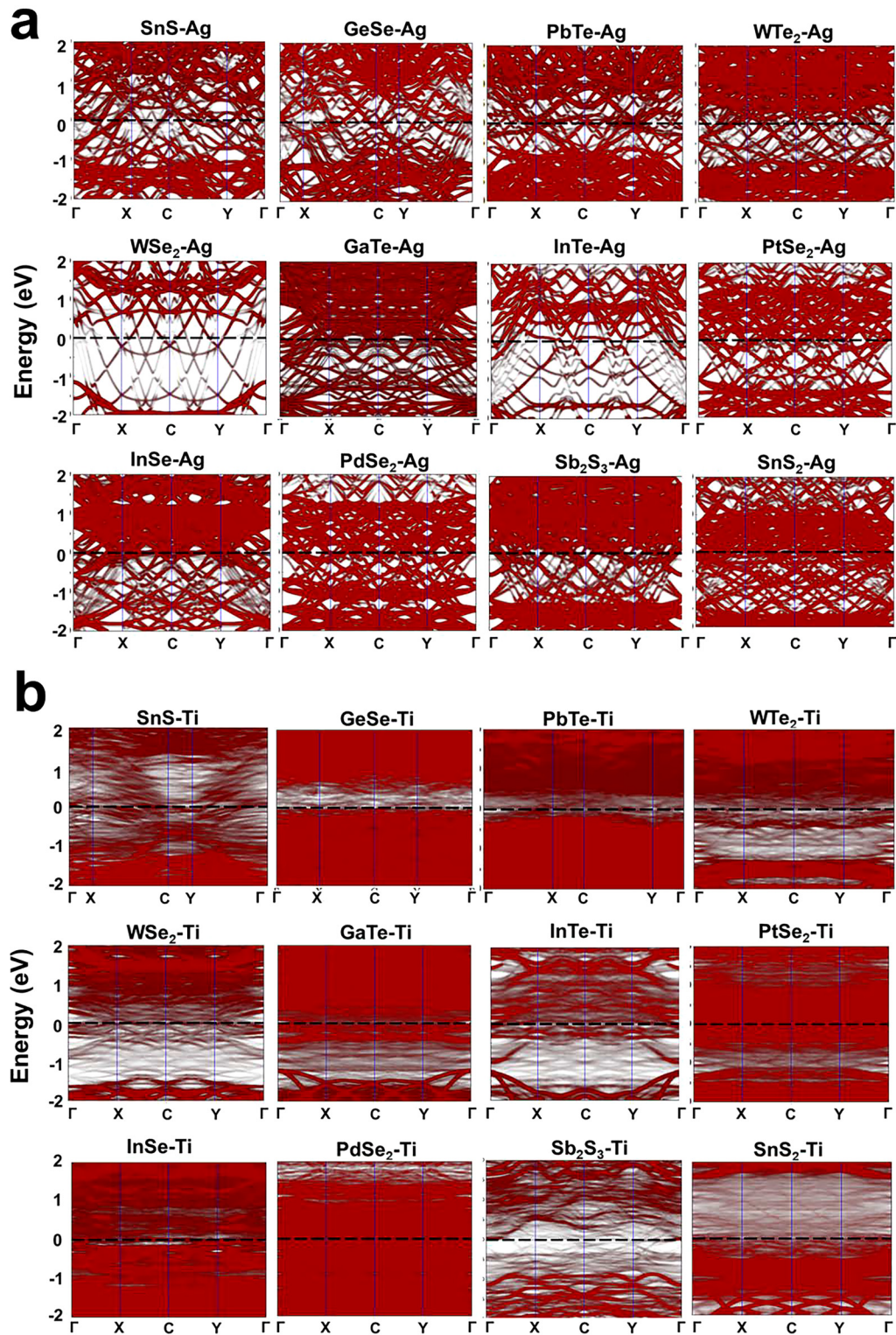


FIG. 3. Projected band structures of 2D materials (colored in red) in (a) 2D SC-Ag and (b) 2D SC-Ti interfaces. The black dashed line denotes the FL.

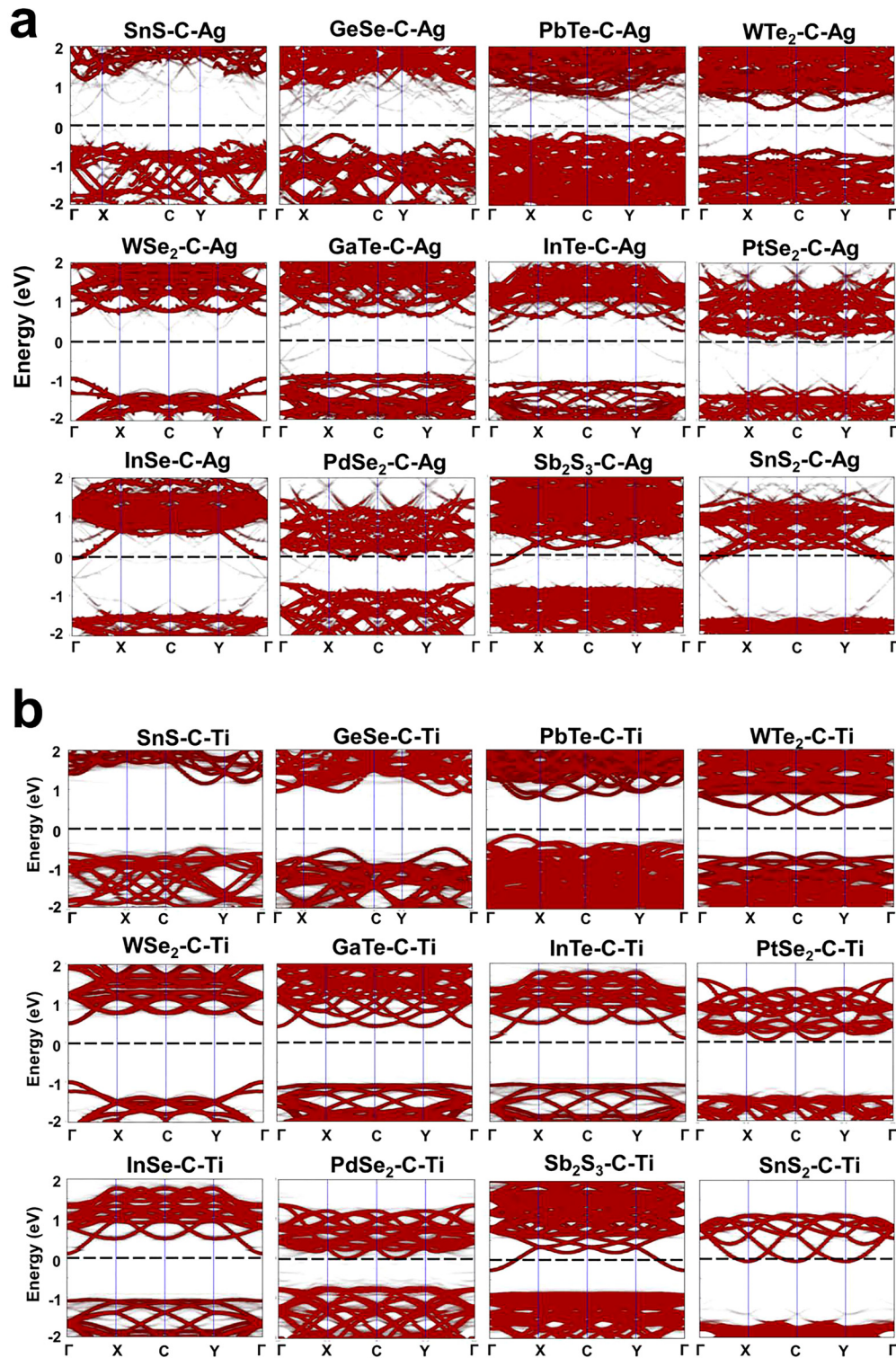


FIG. 4. Projected band structures of 2D materials (colored in red) in (a) 2D SC-graphene-Ag and (b) 2D SC-graphene-Ti interfaces.

height calculated using the two methods is nearly equal. For the rest of the five materials, PtSe₂, InSe, PdSe₂, Sb₂S₃, and SnS₂, both methods show a shifting of FL in the conduction band region, creating Ohmic contacts with zero barrier heights.

2. Barrier analysis in 2D SC-graphene-Ti heterostructures

The comparison between the Schottky barriers in 2D SC-graphene-Ti contacts calculated in the two methods is shown in Fig. 5(b). For all the materials except tellurene, the majority carrier polarities are the same in both methods. Similar to Ag, the values of the electron and hole SBH for SnS and GeSe contacted with graphene-Ti are nearly equal in two methods. For PbTe, the hole SBH obtained from band analysis is about 0.34 eV lower than that calculated from the SM rule. In case of WTe₂, the hole SBH are almost similar in both methods while a small difference of about 0.15 eV is observed in the electron SBH. Like graphene-Ag, the barrier polarity in tellurene-graphene-Ti contact is reversed in the two methods. Band structure analysis shows a p-type contact with smaller hole SBH (0.6 eV) and larger electron SBH (0.7 eV), while

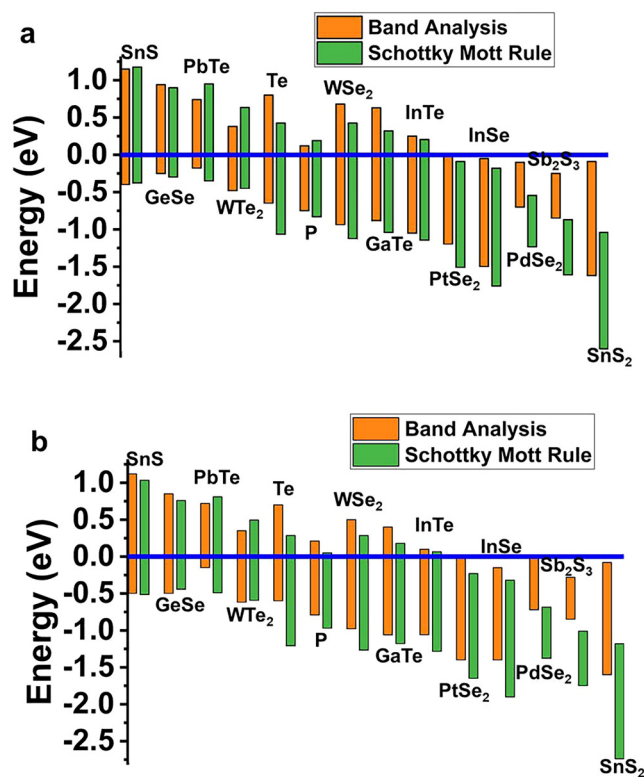


FIG. 5. Comparisons of the SBH in (a) 2D SC-graphene-Ag and (b) 2D SC-graphene-Ti heterostructures calculated using band analysis and the SM rule. The bars represent the energy regions from CBM to VBM in 2D SC in the heterostructures. The blue line corresponds to the FL of the 2D SC-graphene-metal heterostructures.

the SM rule suggests an n-type contact with larger hole SBH (1.2 eV) and smaller electron SBH (0.29 eV). The values of electron SBH obtained for phosphorene, WSe₂, GaTe, and InTe using band analysis are slightly larger compared to SM calculations. For the rest of the five materials, both methods show Ohmic contact formation with zero electron SBH.

Therefore, except for the barrier polarity reversal in one or two cases, the SM rule is followed when 2D materials are contacted with graphene inserted Ag and Ti surfaces. The minor discrepancies in the barrier height occur due to interlayer charge transfer. Even a very small charge transfer can create an interface dipole that cannot be neglected. Due to the formation of such small interface dipoles, the barrier heights vary from the ideal values calculated from the SM rule. The dipole formation between the 2D SC-graphene interfaces can be determined by the electron localization function (ELF). ELF is a tool to identify electron localization in molecular systems. The ELF is formulated by Becke and Edgecombe,⁴⁵ who associated the localization of an electron with the probability density for finding a second like-spin electron near a reference point. For small probability density, the electron is more localized. ELF is a dimensionless quantity that can have values in the range between 0 and 1. ELF = 1 represents perfect localization, whereas ELF = 0.5 corresponds to an electron gas. If no chemical reaction occurs at the interface, no electrons will be there, hence, the ELF value would drop to zero at the interface. However, the nonzero value of ELF is observed at the 2D SC-graphene interface due to the induced dipole interactions (Fig. S2 in the supplementary material). We have found that for Ag and Ti both, the barrier polarity reversal occurs in tellurene. So, we compare the ELF of the tellurene-graphene interface with another material like SnS-graphene, for which the barrier height matches the ideal values (Fig. S2 in the supplementary material). A larger value of ELF at the touching point between C and 2D SC denotes stronger interactions. For the tellurene-graphene interface, the ELF value at the touching point is 0.079 while for the SnS-graphene interface it is 0.045. Hence the dipole formation in tellurene-graphene interface is more than SnS-graphene; as a result, the barrier properties of tellurene deviate from the ideal values. However, the nature of the contact, whether Schottky or Ohmic, can accurately be predicted from the SM rule for all the examined 2D materials.

3. Barrier analysis in 2D SC-graphene-Au (Pd/Pt) heterostructures

To further check whether the SM rule is valid for other metals also, we have made heterostructures by inserting graphene between some of the 2D SCs and higher WF metals like Au, Pd, and Pt. The WFs of graphene-Au, graphene-Pd, and graphene-Pt systems are 5.18, 5.29, and 5.66 eV respectively. In Fig. 6, the comparisons of the obtained barrier using the DFT band analysis and the SM rule are shown. To make interfaces with graphene-Au [Fig. 6(a)], graphene-Pd [Fig. 6(b)], and graphene-Pt [Fig. 6(c)] surfaces, four materials, tellurene, InTe, InSe, and PtSe₂, have been selected. Band structure analysis shows tellurene forms p-type Schottky contacts with all the three metals with barrier heights 0.32, 0.19, and 0.12 eV, respectively. The SM rule predicts the formation of p-type Schottky contacts with Au and Pd, while an Ohmic contact with

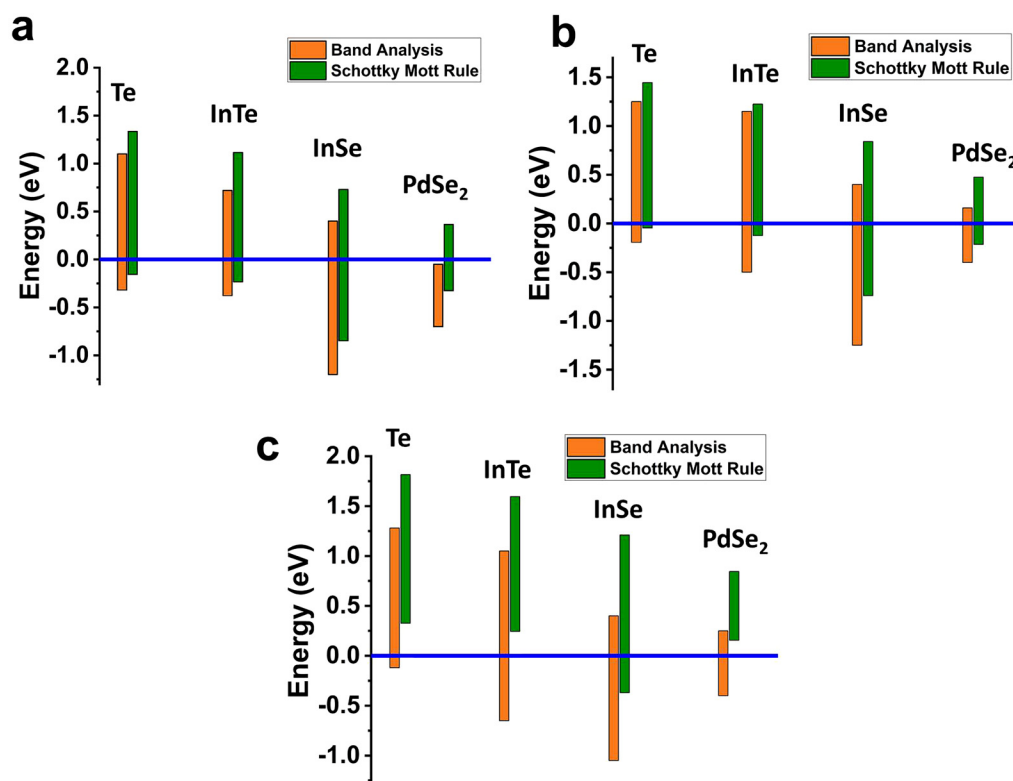


FIG. 6. Comparisons of the SBH in (a) 2D SC-graphene-Au, (b) 2D SC-graphene-Pd, and (c) 2D SC-graphene-Pt heterostructures calculated using band analysis and the SM rule. The bars represent the energy regions from CBM to VBM in 2D SC in the heterostructures. The blue line corresponds to the FL of the 2D SC-graphene-metal heterostructures.

Pt. The barrier heights are slightly different from the calculated values. InTe forms p-type contacts with graphene-Au and graphene-Pd surfaces in both methods. The hole SBH for the graphene-Au interface is about 0.15 eV and for the graphene-Pd interface is about 0.38 eV. The barrier heights are higher in band analysis than SM values. For the InTe-graphene-Pt interface, the SM rule predicts the creation of the Ohmic contact as the WF of the graphene-Pt system is higher than the VBM energies of InTe. However, band analysis shows the formation of the p-type Schottky contact with a sufficiently large barrier of about 0.65 eV. According to band analysis for all three metal surfaces, the FLs shift toward the conduction band of InSe, creating an n-type Schottky contact with the same barrier height of 0.4 eV. According to the SM rule, InSe forms an n-type contact with the graphene-Au surface having a barrier height of about 0.73 eV, while a p-type contact would be formed for Pd and Pt with hole SBH about 0.78 and 0.37 eV, respectively. PdSe₂ band structure analysis shows that when it is interfaced with the graphene-Au surface, the FL crosses the conduction band, creating the Ohmic contact. However, the SM rule predicts valence band maxima come close to the FL making a p-type contact with hole SBH about 0.33 eV. In case of contact with the graphene-Pd surface, the barrier polarity is reversed in the two methods. Band analysis shows an n-type contact with smaller

electron SBH of 0.16 and larger hole SBH of 0.4 eV. The SM theory predicts a p-type contact with larger electron SBH of 0.47 and smaller hole SBH of 0.21 eV. In the case of the graphene-Pt surface, the FL comes near the conduction band of PdSe₂ creating an n-type contact with a barrier of 0.25 eV. But, according to the SM rule, the contact should be Ohmic.

In the case of InSe, the barrier height varies when we increase the WF of metals from 4.49 (Ti) to 5.19 eV (Au). But further increasing the metal's WF, the barrier height does not change, suggesting FLP at the InSe-graphene interface. If the barrier properties of the four SCs contacted with graphene-Au, graphene-Pd, and graphene-Pt surfaces are compared, a significant difference from the SM theory is found in the case of the graphene-Pt interface. To find out the reason behind the discrepancy, we have calculated the ELF_s for graphene-Ag, graphene-Ti, and graphene-Pt interfaces (Fig. S3 in the [supplementary material](#)). Due to the chemical interactions between graphene and Ti, the ELF value at their interfaces is higher than that of the other graphene-metal interfaces. However, for the graphene-Pt interface, the difference between the peak values at graphene and Pt is reduced compared to the other metals. Therefore, it can be said that the electrons of graphene become delocalized with respect to Pt. As the delocalization increases, the chemical reaction between SC and graphene is more probable, causing significant FLP.

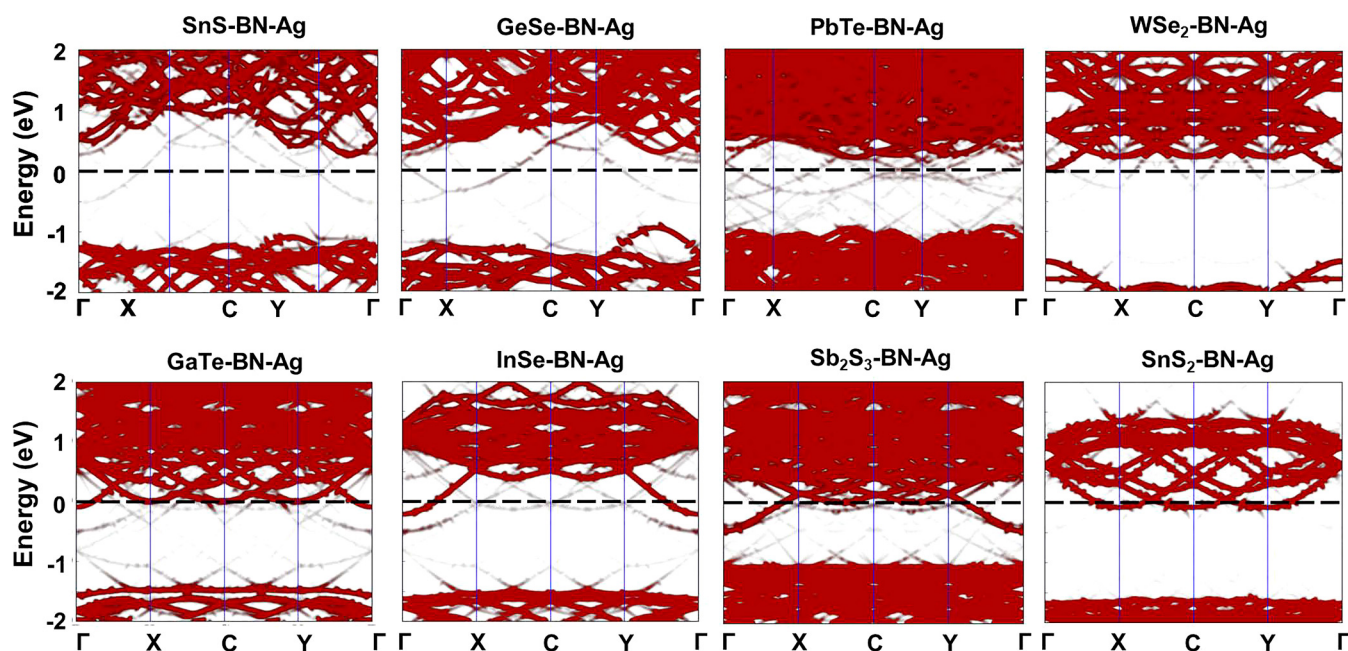


FIG. 7. Projected band structures of 2D materials (colored in red) in 2D SC-h-BN-Ag systems.

D. h-BN insertion

Furthermore, we have evaluated h-BN insertion between 2D SCs and metal interfaces and compared the effect of FL depinning with the graphene inserted structures. Eight SC and two metals Ag and Ti are selected. The projected band structures of 2D SCs in SC-h-BN-Ag heterostructures are shown in Fig. 7. Like graphene, h-BN prevents the metallization of 2D materials and restores their semiconducting band structures. However, except InSe, Sb_2S_3 , and SnS_2 , the barrier properties of other 2D SCs differ from graphene inserted systems. For SnS, GeSe, and PbTe, h-BN insertion creates an n-type Schottky contact, and for WSe_2 and GaTe Ohmic contacts are formed. However, for graphene inserted systems, SnS, GeSe, and PbTe create p-type and WSe_2 and GaTe create n-type contacts. The barrier heights are also different.

Figure 8 shows the comparison between the barriers obtained from DFT band calculations and the SM rule in SC-h-BN-Ag heterostructures. In the two methods, large deviations are found in the barrier nature and heights. From band analysis, it is found that in case of SnS, GeSe, and PbTe, the FLs come near the conduction band creating an n-type Schottky contact with a barrier height of 0.25, 0.29, and 0.2 eV, respectively. However, according to the SM rule, the WF of the h-BN-Ag system (4.39 eV) is close to the VBM, hence a p-type contact should be formed. Band diagrams show that when the rest of the five SCs WSe_2 , GaTe, InSe, Sb_2S_3 , and SnS_2 are contacted with the h-BN-Ag surface the FLs cross their conduction bands creating an Ohmic contact. However, for WSe_2 and GaTe, the SM rule predicts the formation of an n-type Schottky contact with a barrier height of 0.55 and 0.44 eV, respectively. For the other three materials, the SM rule also predicts an Ohmic contact. h-BN

insertion between 2D materials and Ti interfaces also gives similar barrier nature with a minor change in SBH (Fig. S4 in the supplementary material).

In most materials, the barrier properties significantly vary from ideal values if h-BN is used as a buffer layer instead of graphene. From the ELF analysis, we found that the peak value of ELF of h-BN is lower than graphene (Fig. S5 in the supplementary

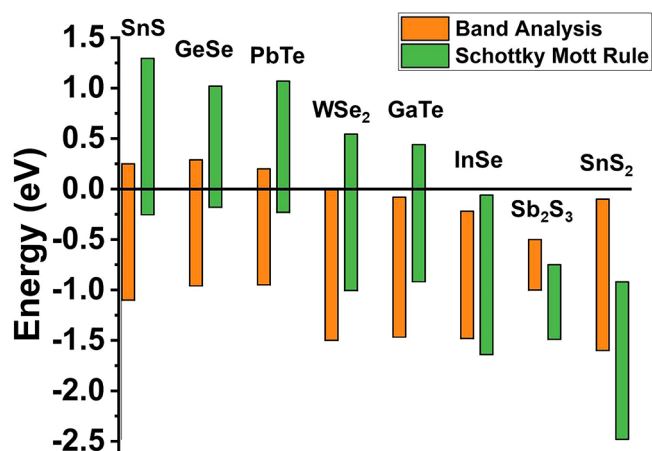


FIG. 8. Comparisons of the SBH in 2D SC-h-BN-Ag heterostructures calculated using projected band analysis and the SM rule. The black line corresponds to the FL of the 2D SC-h-BN-Ag heterostructures.

material). Therefore, the electrons in h-BN are more delocalized, resulting in stronger interactions with the 2D SC surface. Due to stronger chemical reactions between SC and h-BN the barrier properties significantly vary from the SM theory. The traditional quantitative measurement method of FL depinning¹⁷ is not possible here as we have fixed the electrode and varied the semiconductor WFs. As the bandgaps of the semiconducting materials differ, we cannot obtain a linear change in SBH by changing the SC WF. Therefore, we cannot measure the FLP factor¹⁷ for each 2D material. However, we can comment on the level of depinning from the comparisons performed between the DFT calculated, and the SM theory predicted results. Analyzing the above results, we found that when graphene is used as a buffer layer for contacting Ag or Ti electrodes, the depinning of FL is maximum. Although h-BN can shield the chemical interactions between 2D SC and metal, it cannot de-pin the FL well for Ag/Ti electrodes. Also, the depinning effect gets reduced when graphene is interfaced with the Pt electrode. The WFs of ML graphene and h-BN are 4.47 and 3.68 eV, respectively. The WFs of Ag, Ti, and Pt are 4.50, 4.49, and 5.65 eV, respectively. The WF of graphene is nearly the same as the Ag and Ti WF, while Pt has a much

higher WF. It is found that a significant WF difference between the buffer layer and the metal electrode can perturb the electron localization of the buffer layer, as a result, more deviations from the SM rule occur. Therefore, the buffer layer and metal electrodes having near WFs may lead to better depinning of FL.

E. Mulliken analysis

To evaluate charge transfers between the interfaces, we have calculated Mulliken charges⁴⁶ for two materials (SnS and SnS₂) contacted with pure metals and buffer layer inserted metals. The Mulliken charges of SC atoms before and after forming contacts are given in Table S2 in the [supplementary material](#). When SnS is contacted with pure Ag and Ti, it is found that there is significant electron transfer from metal atoms to the nearest Sn and S atoms. The change in Mulliken charges for Ti contacted atoms is much higher than Ag, implying strong chemical reactions. The charge transfer significantly reduces as the buffer layer is inserted, lowering FLP. In SnS–Ag, the average change in Mulliken charge in contacted Sn atoms is about -0.174 e, whereas inserting graphene or

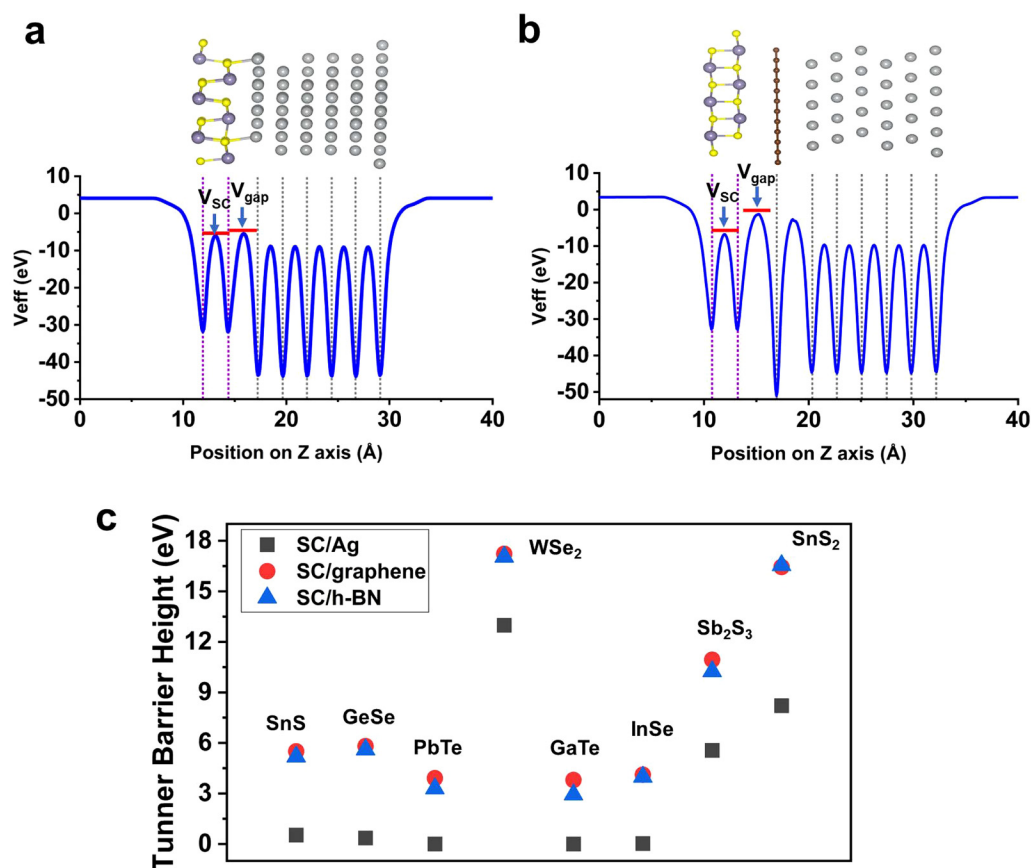


FIG. 9. Plot of average effective potential (V_{eff}) vs z positions in (a) SnS–Ag and (b) SnS–graphene–Ag contacts. Effective tunnel barrier height (ϕ_{TB}) is calculated as $\phi_{\text{TB}} = V_{\text{gap}} - V_{\text{SC}}$. (c) plot of tunnel barrier heights (ϕ_{TB}) for different 2D SCs. The black squares represent ϕ_{TB} in 2D SC–Ag interfaces. The red circles and blue triangles specify ϕ_{TB} in 2D SC–graphene in SC–graphene–Ag systems and 2D SC–h-BN interfaces in SC–h-BN–Ag systems, respectively.

h-BN reduces to about +0.006 and $-0.012 e$, respectively. Similarly, for the SnS₂-Ag interface, the average change in charge in the interface nearest S atoms is about $-0.242 e$. As graphene or h-BN is inserted, it reduces to about -0.70 and $-0.81 e$, respectively. However, the charge transfer in the SC-h-BN interface is more than in the SC-graphene interface, implying that h-BN is more reactive than graphene. As a result, the FLP effect is also higher, leading to deviation from the SM rule.

F. Effect on the tunnel barrier

Inserting a buffer layer introduces an additional tunnel barrier between SC and metal. The tunnel barrier is characterized by its height and width. The effective tunnel barrier height (φ_{TB}) is calculated by taking the difference between average gap potential (V_{gap}) and SC potential (V_{SC}) as shown in Figs. 9(a) and 9(b). The width can be specified by the physical separation between the SC and contacted metal (d_1) or buffer layers (d_2). According to Table I, the distance between the SC and buffer layers (d_2) is larger than that between the SC and metals (d_1), implying an increase in barrier width due to the insertion of graphene or h-BN. The tunnel barrier heights of different SC-Ag contacts and SC-graphene/(h-BN) contacts are shown in Fig. 9(c). Due to chemical reactions, most of the SC-Ag contacts have very low barrier heights. As graphene/(h-BN) is inserted, the tunnel barrier height increases due to weak chemical bonding. For some materials, φ_{TB} is slightly lower in SC-h-BN contacts compared to SC-graphene. This is because chemical reactions between SC and h-BN interfaces are more than that of graphene. Hence, the buffer layer insertion process can significantly reduce the Fermi level pinning in the cost of increasing the tunnel barrier. However, the rise of barrier heights is different for different 2D materials. As shown in Fig. 9(c), φ_{TB} for PbTe and GaTe are lower compared to other materials making them more suitable for contact with graphene/(h-BN). Therefore, the tunnel barrier calculations can provide essential guidelines for selecting efficient 2D semiconductors to form low-resistance Schottky contacts.

IV. CONCLUSIONS

In this work, using rigorous DFT calculations, we have evaluated the electronic properties of heterostructures formed with several 2D SC having a wide range of WFs. We found that all the materials form chemical bonds even with novel metals like Ag. Inserting 2D buffer layers such as graphene or h-BN can shield the chemical interactions between the 2D materials and metals and restore their semiconducting band structures. For most materials, the SM rule is preserved when graphene is interfaced with Ag or Ti metal electrodes. For tellurene-graphene-Ag, WTe₂-graphene-Ag, and tellurene-graphene-Ti, the carrier polarity obtained from DFT calculations is different from the SM rule. However, whether the contact is Schottky or Ohmic can accurately be predicted from the SM rule for all the materials. If the electrode material is changed to Pt, the electron localization of graphene is perturbed, as a result the barrier properties significantly differ from SM predicted values. The SM rule is also not followed if graphene is replaced with h-BN. Therefore, it may be said that graphene combined with Ag or Ti electrodes can de-pin the FL to a great extent. This study gives insight into the FL depinning strategy using the buffer layer in the

emerging 2D materials. Selecting a suitable combination of the buffer layer and metal electrodes, the chemical interactions at the SC interface can be shielded significantly and, hence, the depinning of FL can be enhanced. If the depinning is at maximum, then the barrier properties of new 2D materials can be predicted simply by calculating the bandgap and the WF of the material. This study is highly beneficial in selecting 2D materials, buffer layers, and metal electrodes for high-performance Schottky device fabrication.

SUPPLEMENTARY MATERIAL

See the [supplementary material](#) for details of interface building of 2D-metal and 2D-graphene-metal (Ag/Ti), comparison of the calculated WF and bandgaps with theoretical value, the projected band structure of graphene in GeSe-C-Ag and GeSe-C-Ti, electron localization functions, the Schottky barrier analysis of 2D SC-h-BN-Ti heterostructures, and Mulliken charge analysis.

ACKNOWLEDGMENTS

This work was supported by the Mathematical Research Impact Centric Support (MATRICS) scheme of Science and Engineering Research Board (SERB), Government of India, under Grant No. MTR/2019/000047. S. Mitra acknowledges IISc Institute of Eminence (IOE) postdoctoral fellowship for financial support.

AUTHOR DECLARATIONS

Conflict of Interests

The authors have no conflicts to disclose.

Author Contributions

Sanchali Mitra: Formal analysis (lead); Investigation (lead); Methodology (lead); Validation (lead); Writing – original draft (lead); Writing – review & editing (lead). **Santanu Mahapatra:** Conceptualization (lead); Funding acquisition (lead); Supervision (lead); Writing – original draft (supporting); Writing – review & editing (supporting).

DATA AVAILABILITY

The data that support the findings of this study are available within the article and its supplementary material. Other relevant data are available from the corresponding author upon reasonable request.

REFERENCES

- ¹K. S. Novoselov *et al.*, “Electric field effect in atomically thin carbon films,” *Science* **306**, 666–669 (2004).
- ²M. Zeng, Y. Xiao, J. Liu, K. Yang, and L. Fu, “Exploring two-dimensional materials toward the next-generation circuits: From monomer design to assembly control,” *Chem. Rev.* **118**, 6236–6296 (2018).
- ³W. Cao *et al.*, “2-D layered materials for next-generation electronics: Opportunities and challenges,” *IEEE Trans. Electron Devices* **65**, 4109–4121 (2018).
- ⁴C. Liu *et al.*, “Two-dimensional materials for next-generation computing technologies,” *Nat. Nanotechnol.* **15**, 545–557 (2020).
- ⁵Y. Xu *et al.*, “Contacts between two- and three-dimensional materials: Ohmic, Schottky, and p–n heterojunctions,” *ACS Nano* **10**, 4895–4919 (2016).

- ⁶D. S. Schulman, A. J. Arnold, and S. Das, "Contact engineering for 2D materials and devices," *Chem. Soc. Rev.* **47**, 3037–3058 (2018).
- ⁷Y. Zheng, J. Gao, C. Han, and W. Chen, "Ohmic contact engineering for two-dimensional materials," *Cell Rep. Phys. Sci.* **2**, 100298 (2021).
- ⁸S. B. Mitta *et al.*, "Electrical characterization of 2D materials-based field-effect transistors," *2D Mater.* **8**, 012002 (2020).
- ⁹H. Tian *et al.*, "Novel field-effect Schottky barrier transistors based on graphene-MoS₂ heterojunctions," *Sci. Rep.* **4**, 5951 (2014).
- ¹⁰Y. Wang *et al.*, "Schottky barrier heights in two-dimensional field-effect transistors: From theory to experiment," *Rep. Prog. Phys.* **84**, 056501 (2021).
- ¹¹Y. Kim *et al.*, "Improved sensitivity in Schottky contacted two-dimensional MoS₂ Gas sensor," *ACS Appl. Mater. Interfaces* **11**, 38902–38909 (2019).
- ¹²S. Das *et al.*, "Transistors based on two-dimensional materials for future integrated circuits," *Nat. Electron.* **4**, 786–799 (2021).
- ¹³X. Liu, M. S. Choi, E. Hwang, W. J. Yoo, and J. Sun, "Fermi level pinning dependent 2D semiconductor devices: Challenges and prospects," *Adv. Mater.* **34**, 2108425 (2021).
- ¹⁴K. Soththewes *et al.*, "Universal Fermi-level pinning in transition-metal dichalcogenides," *J. Phys. Chem. C* **123**, 5411–5420 (2019).
- ¹⁵C. Gong, L. Colombo, R. M. Wallace, and K. Cho, "The unusual mechanism of partial Fermi level pinning at metal–MoS₂ interfaces," *Nano Lett.* **14**, 1714–1720 (2014).
- ¹⁶Q. Wang, Y. Shao, P. Gong, and X. Shi, "Metal–2D multilayered semiconductor junctions: Layer-number dependent Fermi-level pinning," *J. Mater. Chem. C* **8**, 3113–3119 (2020).
- ¹⁷R.-S. Chen, G. Ding, Y. Zhou, and S.-T. Han, "Fermi-level depinning of 2D transition metal dichalcogenide transistors," *J. Mater. Chem. C* **9**, 11407–11427 (2021).
- ¹⁸H. Tang *et al.*, "Schottky contact in monolayer WS₂ field-effect transistors," *Adv. Theory Simul.* **2**, 1900001 (2019).
- ¹⁹A. Chanana and S. Mahapatra, "Prospects of zero Schottky barrier height in a graphene-inserted MoS₂-metal interface," *J. Appl. Phys.* **119**, 014303 (2016).
- ²⁰Y. Du *et al.*, "MoS₂ field-effect transistors with graphene/metal heterocontacts," *IEEE Electron Device Lett.* **35**, 599–601 (2014).
- ²¹S.-S. Chee *et al.*, "Lowering the Schottky barrier height by graphene/Ag electrodes for high-mobility MoS₂ field-effect transistors," *Adv. Mater.* **31**, 1804422 (2019).
- ²²J. Wang *et al.*, "High mobility MoS₂ transistor with low Schottky barrier contact by using atomic thick h-BN as a tunneling layer," *Adv. Mater.* **28**, 8302–8308 (2016).
- ²³J. Su, L. Feng, Y. Zhang, and Z. Liu, "The modulation of Schottky barriers of metal–MoS₂ contacts via BN–MoS₂ heterostructures," *Phys. Chem. Chem. Phys.* **18**, 16882–16889 (2016).
- ²⁴J. Su, L. Feng, W. Zeng, and Z. Liu, "Controlling the electronic and geometric structures of 2D insertions to realize high performance metal/insertion–MoS₂ sandwich interfaces," *Nanoscale* **9**, 7429–7441 (2017).
- ²⁵K. Khan *et al.*, "Recent developments in emerging two-dimensional materials and their applications," *J. Mater. Chem. C* **8**, 387–440 (2020).
- ²⁶S. Sucharitakul *et al.*, "Screening limited switching performance of multilayer 2D semiconductor FETs: The case for SnS," *Nanoscale* **8**, 19050–19057 (2016).
- ²⁷T. Das *et al.*, "Doping-free all PtSe₂ transistor via thickness-modulated phase transition," *ACS Appl. Mater. Interfaces* **13**, 1861–1871 (2021).
- ²⁸T. A. Ameen, H. Ilatikhameneh, G. Klimeck, and R. Rahman, "Few-layer phosphorene: An ideal 2D material for tunnel transistors," *Sci. Rep.* **6**, 28515 (2016).
- ²⁹Y. Wang *et al.*, "Field-effect transistors made from solution-grown two-dimensional tellurene," *Nat. Electron.* **1**, 228–236 (2018).
- ³⁰S. Mitra, O. Kesharwani, and S. Mahapatra, "Ohmic-to-Schottky conversion in monolayer tellurene–metal interface via graphene insertion," *J. Phys. Chem. C* **125**, 12975–12982 (2021).
- ³¹Y. Pan *et al.*, "Monolayer phosphorene–metal contacts," *Chem. Mater.* **28**, 2100–2109 (2016).
- ³²S. Li *et al.*, "Interfacial properties of monolayer SnS–metal contacts," *J. Phys. Chem. C* **122**, 12322–12331 (2018).
- ³³P. E. Blöchl, "Projector augmented-wave method," *Phys. Rev. B* **50**, 17953–17979 (1994).
- ³⁴G. Kresse and D. Joubert, "From ultrasoft pseudopotentials to the projector augmented-wave method," *Phys. Rev. B* **59**, 1758–1775 (1999).
- ³⁵G. Kresse and J. Furthmüller, "Efficiency of ab-initio total energy calculations for metals and semiconductors using a plane-wave basis set," *Comput. Mater. Sci.* **6**, 15–50 (1996).
- ³⁶J. P. Perdew, K. Burke, and M. Ernzerhof, "Generalized gradient approximation made simple," *Phys. Rev. Lett.* **77**, 3865–3868 (1996).
- ³⁷J. Moellmann and S. Grimme, "DFT-D3 study of some molecular crystals," *J. Phys. Chem. C* **118**, 7615–7621 (2014).
- ³⁸S. Grimme, S. Ehrlich, and L. Goerigk, "Effect of the damping function in dispersion corrected density functional theory," *J. Comput. Chem.* **32**, 1456–1465 (2011).
- ³⁹H. J. Monkhorst and J. D. Pack, "Special points for Brillouin-zone integrations," *Phys. Rev. B* **13**, 5188–5192 (1976).
- ⁴⁰S. Smidstrup *et al.*, "QuantumATK: An integrated platform of electronic and atomic-scale modelling tools," *J. Phys.: Condens. Matter* **32**, 015901 (2019).
- ⁴¹D. R. Hamann, "Optimized norm-conserving Vanderbilt pseudopotentials," *Phys. Rev. B* **88**, 85117 (2013).
- ⁴²M. Schlupf and F. Gygi, "Optimization algorithm for the generation of ONCV pseudopotentials," *Comput. Phys. Commun.* **196**, 36–44 (2015).
- ⁴³D. Stradi, L. Jelver, S. Smidstrup, and K. Stokbro, "Method for determining optimal supercell representation of interfaces," *J. Phys.: Condens. Matter* **29**, 185901 (2017).
- ⁴⁴R. T. Tung, "The physics and chemistry of the Schottky barrier height," *Appl. Phys. Rev.* **1**, 011304 (2014).
- ⁴⁵A. D. Becke and K. E. Edgecombe, "A simple measure of electron localization in atomic and molecular systems," *J. Chem. Phys.* **92**, 5397–5403 (1990).
- ⁴⁶R. S. Mulliken, "Electronic population analysis on LCAO–MO molecular wave functions. I," *J. Chem. Phys.* **23**, 1833–1840 (1955).